minerals

MDPI

Article

Magnetotelluric Responses of an Anisotropic 1-D Earth with a Layer of Exponentially Varying Conductivity

Linjiang Qin [1,2,*], Weifeng Ding [2] and Changfu Yang [3]

[1] Key Laboratory of Submarine Geosciences, Ministry of Natural Resources, Hangzhou 310012, China
[2] Second Institute of Oceanography, Ministry of Natural Resources, Hangzhou 310012, China; wfding@sio.org.cn
[3] Key Laboratory of Geoscience Big Data and Deep Resource of Zhejiang Province, School of Earth Sciences, Zhejiang University, Hangzhou 310027, China; ycfzju@zju.edu.cn
* Correspondence: qinlinjiang@sio.org.cn; Tel.: +86-571-81969133

Abstract: The magnetotelluric (MT) sounding of a layered Earth model involving a transitional layer has been widely studied, and MT responses of the model with dipping anisotropic conductivity have also been treated. However, a model incorporating both a transitional layer and dipping anisotropy has seldom been considered. The analytical solution of such a geoelectrical model including three layers was derived in this study. The middle layer was a transitional layer with conductivity exponentially varying with depth, which was covered by a homogeneous layer and underlaid by a dipping anisotropic half-space. The electromagnetic (EM) fields in the transitional layer were explicitly solved with modified Bessel functions. The surface impedance was calculated recursively. The dependence of the apparent resistivity and impedance phase as well as the EM fields on different model parameters were investigated in detail. We believe that our analytical solution provides a useful complement to the theory of the one-dimensional (1D) inversion and interpretation based on the layered model with fixed conductivity.

Keywords: magnetotelluric fields; analytical expressions; transitional layer; anisotropy; apparent resistivity; electromagnetic method

Citation: Qin, L.; Ding, W.; Yang, C. Magnetotelluric Responses of an Anisotropic 1-D Earth with a Layer of Exponentially Varying Conductivity. *Minerals* **2022**, *12*, 915. https://doi.org/10.3390/min12070915

Academic Editors: Binzhong Zhou, Changchun Yin, Zhengyong Ren, Xuben Wang and Amin Beiranvand Pour

Received: 16 May 2022
Accepted: 19 July 2022
Published: 21 July 2022

1. Introduction

The magnetotelluric (MT) [1–3] method is a passive geophysical exploration technique for determining the subsurface conductivity structure using natural electromagnetic (EM) fields. With advances in computer technology and numerical techniques, it is now possible to calculate the MT responses of various complex models in two dimensions (2D) and three dimensions (3D) by numerical modelling; thus, many programs have been developed [4–19]. However, although a number of 2D and 3D numerical simulation codes have been developed and applied in many aspects related to MT research, studies on the analytical responses over a one-dimensional (1D) Earth model still have a certain degree of importance in the application of MT techniques, especially in some special circumstances, for example, on the ocean bottom, where, sometimes, not enough MT data are available to conduct 2D or 3D studies, and 1D inversion and interpretation is a necessary technique [20]. Furthermore, a 1D solution may be presented as a technical appendix to a publication presenting a 3D solver, since it is very useful when developing 3D solvers and verifying their accuracy. Additionally, 1D MT is still applied to probe some simple structures such as basin depth [21] and geothermal fields [22–24], and it is also used to understand EM wave propagation in the Earth [25].

Most of the publications on the 1D analytical solutions of MT responses appeared in the 1970s–1980s or earlier. The models considered in these publications may be categorized into two groups: those with sharp boundaries [26–31] and those with transitional boundaries [32–37]. In the former case, the model is composed of several layers with fixed conductivity; while in the latter case, the model includes at least one layer in which the conductivity varies with

depth. From the perspective of practical observation, a number of resistivity well-logging analyses [38–40] have advocated that the boundaries between layers are transitional in nature rather than sharp. Therefore, studies of MT responses to 1D transitional models are important and necessary.

Some authors have reported analytical solutions to the MT fields of 1D transitional models. For instance, Mallick [32] and Kao and Rankin [34] examined the MT responses of an inhomogeneous layered Earth of conductivity linearly varying with depth. Berdichevsky et al. [41] considered the MT responses of models of resistivity exponentially decreasing with depth. Banerjee et al. [37] reported the apparent resistivity of a multilayered Earth with a layer having exponential variation in the conductivity. Kao [35] considered the MT fields of a vertical inhomogeneous model of resistivity varying linearly with depth. Kao [36] also presented the MT responses to a 1D model with the conductivity varying exponentially as a function of depth. Kim and Lee [42] investigated the response of a layered Earth of resistivity exponentially varying with depth. Pal [43] examined the MT responses over a 1D Earth with a nonmonotonic resistivity distribution in a transitional layer. Additionally, Berdichevsky and Dmitriev [44] summarized the analytical solutions of two special cases of gradient models, i.e., the Dmitriev–Kao model [36,41] and the Kato–Kikuchi model [45], which are characterized by exponentially varying conductivity with depth. Qin and Yang [46] calculated the MT responses over a layered model containing two transitional layers.

However, these previously mentioned models did not involve anisotropy. There have been some studies in which the model involved electrical anisotropy. For example, Negi and Saraf [47] reported the MT sounding of a layered model with a transitional layer underlaid by a dipping anisotropic half-space in which the conductivity in the transition layer varied linearly with depth. Kovacikova and Pek [48] presented generalized Riccati equations for 1D MT impedances of electrical anisotropic structures. Recently, Qin et al. [49] published the MT responses of a 1D resistivity structure model involving anisotropic transitional layers.

In this study, we extended the work of Negi and Saraf [47] to a case where the conductivity varied exponentially with depth in the transitional layer. Although this model is a very specific setting, it is still necessary and important to consider. The first layer may represent the shallow sediment layer. The transitional layer can describe a frozen surface layer [50] or the zone of weathered rock [51]. For the bottom layer with uniaxial anisotropy, the plane of anisotropy makes an angle with the horizontal interface between the transitional layer and the basement; such an interface may behave as a plane of unconformity between two sedimentary strata (a typical stratigraphic trap, which is favourable for the accumulation of oil), therefore, an analysis of the MT responses to such a model is expected to be beneficial for oil exploration [52]. Moreover, it is well known that the transitional layer can be approximately equivalent to numbers of thin layers that have fixed conductivities with depth [46,53], and further numerical approaches can be adopted to obtain the MT responses. However, as stated by Chlamtac and Abramovici [50], when the calculation is considered in inverse problems, the number of parameters to be determined using this three-layer model is largely fewer than that using a stack of thin layers and thus simplifies the problem.

The rest of this work is arranged as follows: the model and its MT responses are demonstrated in Section 2. After that, the validation of the algorithm is presented in Section 3. Next, in Section 4, the variation in the MT responses with the model parameters is illustrated. Finally, the conclusions are given in Section 5.

2. Model and Formulations

2.1. The Vertical Inhomogeneous and Anisotropic Model

For the problem considered in the following texts, a plane EM wave with the time factor $e^{i\omega t}$ (ω and t are the angular frequency and time, respectively; i is the imaginary unit and $i = \sqrt{-1}$) is assumed. The 1D layered model to be treated is shown in Figure 1. The model is composed of two different media: the isotropic medium (the first and second layers) and the anisotropic medium in the base (the third layer). In addition, the second

layer is a transitional layer with conductivity that varies exponentially with depth. To solve the induction problem in this work, we set up two different coordinate systems: one is *o*-$x'y'z'$ (a Cartesian coordinate system) for the isotropic media, and the other is *o*-*xyz* for the anisotropic medium in the third layer (a principal axes coordinate system). Just to make the model clear, the coordinate systems are represented by black axes and the conductivity parameters are marked by grey axes.

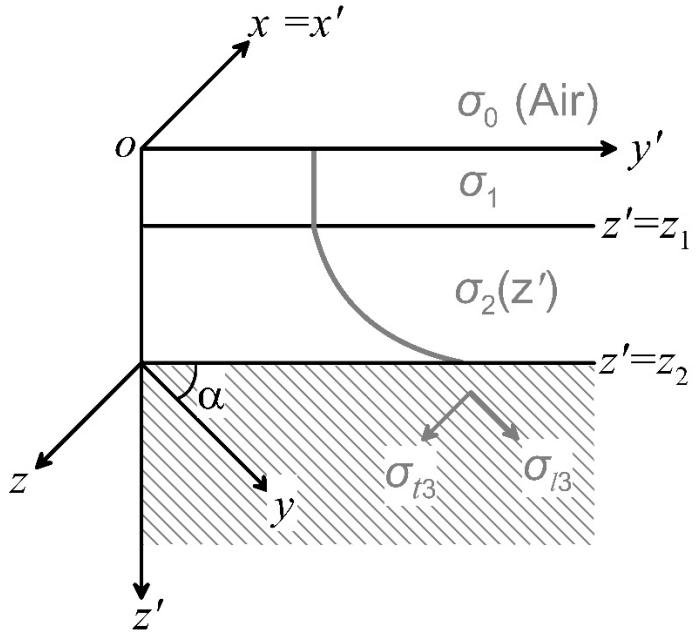

Figure 1. A 1D layered anisotropic model containing three layers. The black axes are for the coordinate system. The top layer is an isotropic layer of fixed conductivity σ_1. The middle layer is a transitional layer of conductivity that varies exponentially with depth, represented by $\sigma_2(z')$. The bottom layer is a dipping anisotropic bed of conductivities σ_{l3} and σ_{t3} in the longitudinal and transverse directions, respectively, in the *o*-*xyz* coordinate system. The variation in conductivity with depth in the top and middle layers are represented by the grey line and the curve, respectively, and the anisotropic conductivities in the bottom layer are marked by grey arrows. The dipping direction of the bottom bed makes an angle α with the horizontal interface.

For simplicity, the problem is treated in Cartesian coordinates, in which the horizontal electric field component $E_{y'}$ and orthogonal horizontal magnetic field $H_{x'}$ are typically to be solved.

The electrical conductivity in the middle layer is assumed to be written as:

$$\sigma_2(z') = \sigma_1 e^{q(z'-z_1)} \tag{1}$$

where z_1 indicates the depth of the interface between the top and middle layers, and q in the exponential power is the rate of the change in conductivity, which may be defined by

$$q = \ln[\sigma_{l3}/(\sigma_1\beta^2)]/(z_2 - z_1) \tag{2}$$

where $\beta^2 = 1+(\lambda^2-1)\sin^2\alpha$, $\lambda = (\sigma_{l3}/\sigma_{t3})^{1/2}$ is the coefficient of anisotropy, the longitudinal conductivity σ_{l3} is parallel to the axis y, the transverse conductivity σ_{t3} is parallel to the axis z, and z_2 is the depth of the lower boundary of the second layer from the surface of the Earth.

Due to the different characteristics of the conductivity in the three layers, Maxwell's equations must be solved in the three layers to calculate the EM fields.

2.2. The EM Fields in the Top Layer

The displacement current is usually ignored for MT soundings; thus, the Helmholtz equation to be satisfied in the isotropic layer may be written as [47,54,55]:

$$\frac{d^2E_{y'1}}{dz'^2} - k_1^2 E_{y'1} = 0 \tag{3}$$

where $k_1 = \sqrt{i\omega\mu\sigma_1}$ defines the propagation constant of the EM wave, μ is the magnetic permeability and $E_{y'1}$ is the horizontal electric field in the top layer.

The general solution to Equation (3) is given by the following formula [56]:

$$E_{y'1} = Ae^{-k_1 z'} + Be^{k_1 z'} \tag{4}$$

where A and B are undetermined coefficients to be found by applying the boundary conditions.

Once the electric field has been obtained, the horizontal magnetic field component can be easily obtained using the following formula from Maxwell's equations:

$$H_{x'1} = \frac{1}{i\omega\mu}\frac{\partial E_{y'1}}{\partial z'} \tag{5}$$

By combining Equations (4) and (5), the horizontal magnetic field component is given by:

$$H_{x'1} = \frac{k_1}{i\omega\mu}\left(-Ae^{-k_1 z'} + Be^{k_1 z'}\right) \tag{6}$$

2.3. The EM Fields in the Middle Layer

The Helmholtz's equation governing EM induction in the middle layer is expressed as:

$$\frac{d^2E_{y'2}}{dz'^2} - k_2^2 E_{y'2} = 0 \tag{7}$$

where $k_2 = \sqrt{i\omega\mu\sigma_2(z')}$ is the propagation constant (varying with the depth) in the region of 2 and $E_{y'2}$ represents the corresponding horizontal electric field component.

Substitution of Equation (1) into (7) yields:

$$\frac{d^2E_{y'2}}{dz'^2} - i\omega\mu\sigma_1 e^{q(z'-z_1)}E_{y'2} = 0 \tag{8}$$

Now, we introduce a new variable γ, which is defined as:

$$\gamma = 2\sqrt{i\omega\mu\sigma_1 e^{q(z'-z_1)}}/q \tag{9}$$

Thus, the first-order derivative of γ is obtained from Equation (9):

$$\frac{d\gamma}{dz'} = \sqrt{i\omega\mu\sigma_1 e^{q(z'-z_1)}} \tag{10}$$

Subsequently, combining Equations (8)–(10) yields a second-order differential equation of $E_{y'2}$ for the variable γ:

$$\frac{d^2E_{y'2}}{d\gamma^2} + \frac{1}{\gamma}\frac{dE_{y'2}}{d\gamma} - E_{y'2} = 0 \tag{11}$$

Clearly, Equation (11) is a modified Bessel equation of zero order, and its general solution has the following form [57]:

$$E_{y'2} = CI_0(\gamma) + DK_0(\gamma) \tag{12}$$

where $I_0(\gamma)$ and $K_0(\gamma)$ are the modified Bessel functions of the first and second type of order zero, respectively, and C and D are undetermined coefficients to be evaluated by applying the boundary conditions.

Next, the horizontal magnetic field component $H_{x'2}$ is examined by Equation (12) with the help of $I_0'(\gamma) = I_1(\gamma)$ and $K_0'(\gamma) = -K_1(\gamma)$, and the derivative of $E_{y'2}$ with respect to z' can be written as a function of γ thanks to Equation (10):

$$\begin{aligned} H_{x'2} &= \frac{1}{i\omega\mu}\frac{\partial E_{y'2}}{\partial z'} = \frac{1}{i\omega\mu}\frac{dE_{y'2}}{d\gamma}\sqrt{i\omega\mu\sigma_1 e^{q(z'-z_1)}} \\ &= \frac{\sqrt{i\omega\mu\sigma_1 e^{q(z'-z_1)}}}{i\omega\mu}[CI_1(\gamma) - DK_1(\gamma)] \end{aligned} \tag{13}$$

2.4. The EM Fields in the Bottom Layer

The EM fields in a dipping anisotropic medium have been previously investigated [52,58]; these results were used in this study. Thus, the horizontal magnetic field component $H_{x'3}$ in the bottom layer is given by the following expression:

$$H_{x3} = H_{x'3} = Fe^{-k_3 z'} = Fe^{-k_3(z\cos\alpha + y\sin\alpha)} \tag{14}$$

where $k_3 = \sqrt{i\omega\mu\sigma_{l3}/\beta^2}$ is the propagation constant in the bottom layer, and F is an undetermined coefficient to be estimated by applying boundary conditions.

From Maxwell's equation, the horizontal electric field can be related to the horizontal magnetic component in the dipping anisotropic medium via the following expressions [52,58]

$$\begin{cases} \frac{\partial H_{x3}}{\partial z} = \sigma_{l3}E_{y3} \\ \frac{\partial H_{x3}}{\partial y} = -\sigma_{t3}E_{z3} \end{cases} \tag{15}$$

Substitution of Equation (14) into (15) gives the horizontal and vertical electric components in the bottom layer:

$$\begin{cases} E_{y3} = -\frac{k_3\cos\alpha}{\sigma_{l3}}Fe^{-k_3(z\cos\alpha + y\sin\alpha)} \\ E_{z3} = \frac{k_3\sin\alpha}{\sigma_{t3}}Fe^{-k_3(z\cos\alpha + y\sin\alpha)} \end{cases} \tag{16}$$

Finally, the horizontal electric component $E_{y'3}$ needs to be determined in the Cartesian coordinate system; therefore, a relationship should be established between the Cartesian coordinate system and the principal axes coordinate system. This relationship may be easily seen in Figure 1; that is, $z' = z\cos\alpha + y\sin\alpha$. Hence, the horizontal electric component $E_{y'2}$ may be written as:

$$\begin{aligned} E_{y'3} &= E_{y3}\cos\alpha - E_{z3}\sin\alpha \\ &= \frac{-k_3\beta^2}{\sigma_{l3}}Fe^{-k_3(z\cos\alpha + y\sin\alpha)} \\ &= \frac{-k_3\beta^2}{\sigma_{l3}}Fe^{-k_3 z'} \end{aligned} \tag{17}$$

2.5. Evaluation of Undetermined Coefficients

The electric and magnetic fields in the three layers of the model in Figure 1 have been explicitly examined with several undetermined coefficients (i.e., A, B, C, and D), which were evaluated using the boundary conditions at $z' = z_1$ and $z' = z_2$. The equivalence of the electric and magnetic fields at the two interfaces may be written as follows:

$$\begin{cases} E_{y'1} = E_{y'2} \\ H_{x'1} = H_{x'2} \\ E_{y'2} = E_{y'3} \\ H_{x'2} = H_{x'3} \end{cases} \tag{18}$$

Substitution of Equations (4), (6), (12)–(14) and (17) into Equation (18) yields:

$$\begin{cases} Ae^{-k_1 z_1} + Be^{k_1 z_1} = CI_0(\gamma_1) + DK_0(\gamma_1) \\ -Ae^{-k_1 z_1} + Be^{k_1 z_1} = CI_1(\gamma_1) - DK_1(\gamma_1) \\ CI_0(\gamma_2) + DK_0(\gamma_2) = NFe^{-k_3 z_2} \\ U[CI_1(\gamma_2) - DK_1(\gamma_2)] = Fe^{-k_3 z_2} \end{cases} \tag{19}$$

where $\gamma_1 = \gamma|_{z=z_1} = 2\sqrt{i\omega\mu\sigma_1}/q$, $\gamma_2 = \gamma|_{z=z_2} = 2\sqrt{i\omega\mu\sigma_1 e^{p(z_2-z_1)}}/q$, $N = -\frac{k_3\beta^2}{\sigma_{l3}}$ and $U = \sqrt{\frac{\sigma_1 e^{q(z_2-z_1)}}{i\omega\mu}}$.

The relationships of different unknown coefficients may be obtained from Equation (19) (see the details in Appendix A).

2.6. Apparent Resistivity and Impedance Phase

Once the relationship of the EM fields at the surface of the model has been obtained, the surface impedance can be immediately deduced from the following expression:

$$Z|_{z'=0} = \left.\frac{E_{y'1}}{H_{x'1}}\right|_{z'=0} = \frac{i\omega\mu}{k_1}\frac{1 + A/B}{1 - A/B} \tag{20}$$

where A/B is recursively solved from Equation (19) (see Appendix A for details).

Furthermore, the apparent resistivity ρ_a and the impedance phase φ can be examined using the following expressions:

$$\begin{cases} \rho_a = |Z|^2/\omega\mu \\ \varphi = \tan^{-1}(Z_{\mathrm{Im}}/Z_{\mathrm{Re}}) \end{cases} \tag{21}$$

where Z_{Im} and Z_{Re} represent the imaginary and real parts of the surface impedance, respectively.

3. Validation of the Method

The algorithm presented in the previous section was validated by comparing the apparent resistivity and impedance phase calculated by the method in this work for the 1D model shown in Figure 1 (called the exponential model hereinafter) and results were obtained using the program code Z1ANIS.FOR provided by Pek and Santos [59] (referred to as Pek1DAniCode in the following text; see Appendix B for details) for homogeneous multilayer approximation models (hereafter called the stair-step model). The model parameters of the exponential model are as follows: $\sigma_1 = 0.01$ S/m, $\sigma_{l3} = 0.02$ S/m, $\sigma_{t3} = 0.06$ S/m, $z_1 = 200$ m, $z_2 = 2200$ m, and $\alpha = 30^\circ$. To evaluate the validity of the analytical solution in this study, three stair-step models with steps of 200, 100 and 20 m were designed to approximate the transitional layer in the exponential model. The first and second layers are shown in Figure 2, where the black solid curve represents the exponential model considered in this study, and the magenta, blue and green lines represent the stair-step models with a step of 200, 100 and 20 m, respectively. For the stair-step models, the conductivities of thin layers within the depth of the middle layer in the exponential model were calculated using Equation (1).

For the given model, the apparent resistivity and impedance phase were computed by the method described in Section 2 and by Pek1DAniCode, respectively. The corresponding results are shown in Figure 3. The apparent resistivity of the exponential model is shown by the black solid curve in Figure 3a, while the apparent resistivity of the stair-step models with steps of 200, 100 and 20 m are indicated by magenta, blue and green dashed curves, respectively. Figure 3b shows the impedance phase for the exponential model (black curve) and stair-step models (magenta, blue and green curves).

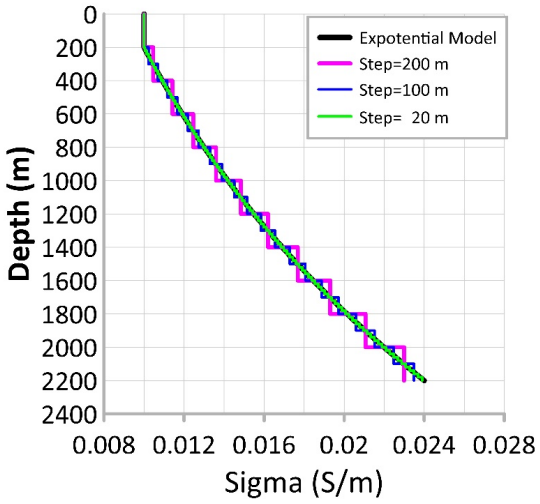

Figure 2. The 1D layered model contains a layer of exponentially varying conductivity (black solid curve) and a stair-step model with steps of 200 m (magenta solid curve), 100 m (blue solid curve) and 20 m (green solid curve). The exponentially varying conductivity model is represented by the "Exponential model" in the legend, and the stair-step model with a step of 200 m is marked as "Step = 200 m" (and similarly for the other stair-step models). Please note that the bottom layer (the anisotropic layer) is not shown in the figure.

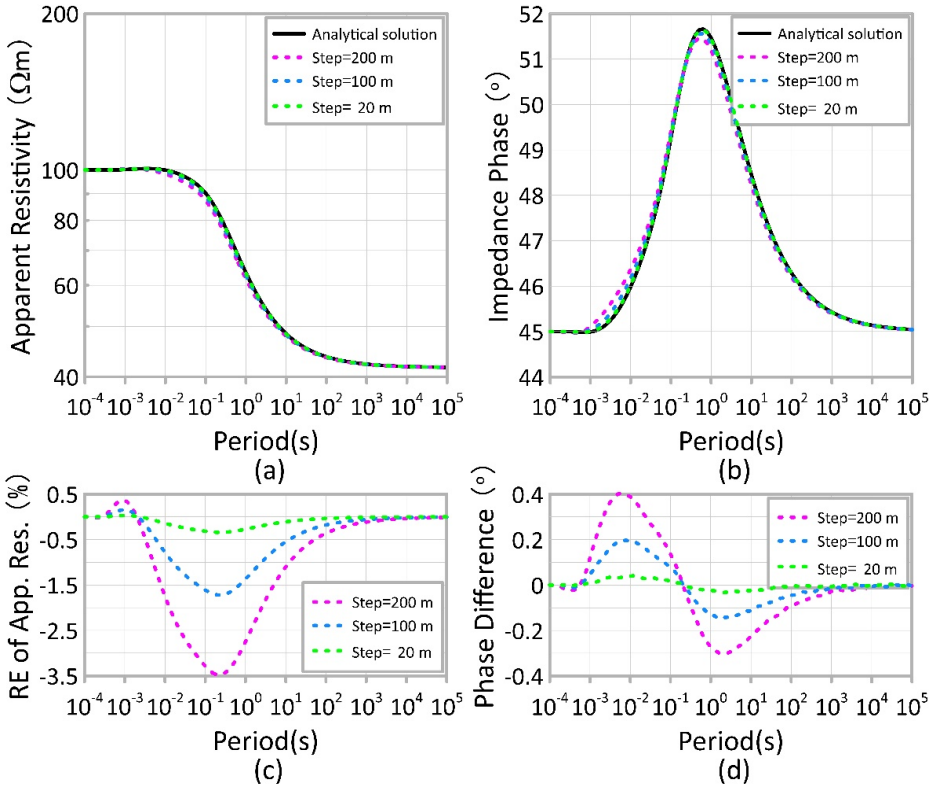

Figure 3. Comparison of the MT soundings given by the algorithm presented in this work for the exponential model denoted by the black solid line shown in Figure 2 and those obtained using the Pek1DAniCode for the stair-step models shown by magenta, blue and green dashed lines in Figure 2. (**a**) Apparent resistivity. (**b**) Impedance phase. (**c**) Relative error (RE) of the apparent resistivity. (**d**) Phase difference (PD). The results calculated using the method in this study are as by "Analytic solution" in the legend, and the results for the stair-step model with a step of 200 m are marked as "Step = 200 m" (and similarly for the other stair-step models). See the text for details.

To evaluate the accuracy of the algorithm in this work, the relative error (RE) of the apparent resistivity of the different models was introduced, and the phase difference (PD) of the models was also evaluated. The formulas used to calculate RE and PD are as follows:

$$\begin{cases} RE = \frac{\rho_{as} - \rho_{ss}}{\rho_{as}} \times 100\% \\ PD = \varphi_{as} - \varphi_{ss} \end{cases} \quad (22)$$

where ρ_{as} and φ_{as} represent the apparent resistivity and impedance of the analytic solution, respectively, and ρ_{ss} and φ_{ss} are the apparent resistivity and impedance of the step-stair models calculated by Pek1DAniCode, respectively.

The RE of the apparent resistivity for the stair-step models with respect to the ones for the exponential model were computed using Equation (22), and the corresponding results are indicated by the magenta, blue and green dashed curves in Figure 3c. The maximum value of RE in the apparent resistivity was approximately −3.5% when the step was 200 m (i.e., the thickness of layers approximating the transitional layer was 200 m), while it decreased to less than 0.5% when the step decreased to 20 m. The phase difference (PD) between the results for the stair-step models and those for the exponential model were also calculated by Equation (22), and the resulting values are represented by the magenta, blue and green dashed curves in Figure 3d. The maximum value of PD was approximately 0.4° when the step was 200 m, while it decreased to less than 0.05° when the step was reduced to 20 m.

Thus, the comparison in Figure 3 clearly shows that the apparent resistivity and impedance phase for the stair-step model obtained with Pek1DAniCode asymptotically converge to the analytical solution of the exponential model with an increasing number of layers (decreasing thickness) approximating the transitional layer. Therefore, the algorithm presented in this study has been validated.

4. Dependence of the Apparent Resistivity and Impedance Phase on the Model Parameters

In this part of the study, the dependence of the apparent resistivity and impedance phase on the model parameters (dip angle, anisotropic coefficient and layer thickness) was investigated.

For the simplicity of analysis, the conductivity in the top layer and the longitudinal conductivity in the bottom layer were kept unchanged ($\sigma_1 = 0.01$ S/m, $\sigma_{l3} = 0.1$ S/m) in the following calculation, and then we considered the variations in MT responses with other parameters (dip angle α, anisotropic coefficient λ and normalized thickness h). The normalized thickness was defined as $h = [(z_2 - z_1) - z_1]/z_1$, and the anisotropic coefficient λ was defined in Section 2.1.

To provide an integrated insight into the influence of various parameters on MT responses, three values were chosen for the anisotropic dip angles ($\alpha = 15°$, 30°, and 60°), and four values were assigned for the anisotropic coefficient ($\lambda = 1$, 2, 3, and 4) in the case of two different normalized thicknesses of the transitional layer ($h = 1$, 2) in the calculation. The results are shown in Figure 4. For the convenience of plotting, dimensionless quantities were adopted. That is, the apparent resistivity normalized by the resistivity of the first layer and the impedance phases were plotted against the normalized skin depth z_1/δ_1, where δ_1 represents the skin depth of the incident EM wave with a given frequency in a half-space with the conductivity value of σ_1. Additionally, it is worth noting that the impedance phase was transformed into the first quadrant.

For given anisotropic coefficients and dip angles, it is clear from the top panels in Figure 4 that as the value of h is increased from 1 to 2, the values of the normalized apparent resistivity increased correspondingly for intermediate values of $z_1/\delta_1(0.1 - 1.0)$, except for the case of $\alpha = 60°$ and $\lambda = 4$, while no difference may be seen for very large (>1.0) or very small values (<0.01) of z_1/δ_1. The bottom panels in Figure 4 show that the impedance phase first increased with an increasing h until it reached the peak value and then decreased with h (except for the case of $\alpha = 60°$ and $\lambda = 4$). It is also obvious that the extremum value of the impedance phase decreased as h increased. A possible explanation for this

phenomenon is that due to the increase in the thickness of the middle layer, more EM energy was attenuated in this layer; thus, the energy reflected from the lower boundary decreased, and a less destructive interference with the incident wave was created in this case.

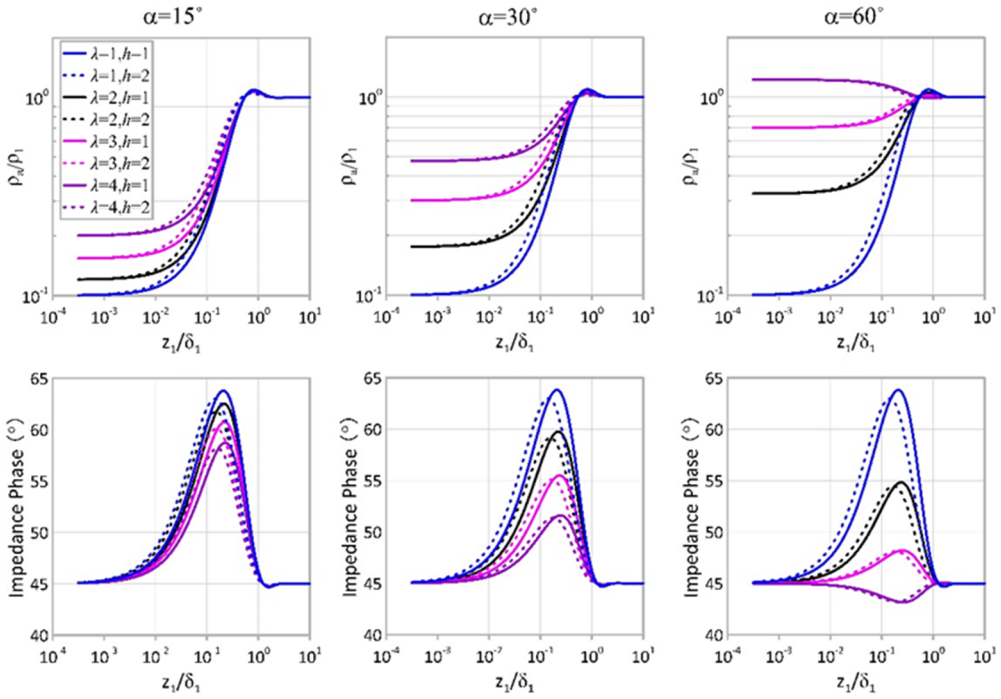

Figure 4. The normalized apparent resistivity (top panels) and impedance phase (bottom panels) at the surface of the vertical inhomogeneous and anisotropic Earth with various model parameters. ρ_1 is the resistivity of the first layer and the inverse of σ_1; $\delta_1 = \sqrt{2/\omega\mu\sigma_1}$ is the skin depth of the incident EM wave with a given frequency and the conductivity in the top layer. The curves presented in the left, middle and right columns correspond to three different dip angles. In each panel, the results for different anisotropic coefficients are marked by curves in different colours, while those for the normalized thicknesses of 1 and 2 are marked by solid and dashed lines, respectively.

For a given anisotropic dip angle, as the value of the anisotropic coefficient (λ) increases, the normalized apparent resistivity and impedance phase change proportionally. These most significant changes appeared in the normalized apparent resistivity for smaller values of z_1/δ_1 (<1) and in the impedance phase for intermediate values of z_1/δ_1 (0.01–1). Additionally, the normalized apparent resistivity and impedance phase are independent of the anisotropic dip angles if the basement layer becomes isotropic (the blue solid or dashed curves marked by $\lambda = 1$ in the legend). The increase in the anisotropic coefficient (λ) implies a decrease (or increase) in the conductivity (resistivity) in the transverse direction, and the EM energy reflected from the third layer increases and may create more constructive interference with the incident EM wave.

For a given anisotropic coefficient (except for $\lambda = 1$), the normalized apparent resistivity increases as h increases; however, the impedance phase shows the opposite characteristic.

5. Discussion: Variations in the EM Fields with Model Parameters

In the previous section, the dependence of the apparent resistivity and impedance phase on the model parameters were investigated. In this section, we discuss how the intensity of the anisotropy and dip angle affect the current and EM fields in each layer. The models considered here are the same as those used in the previous section. The thickness of the top layer is fixed at 500 m, while the thickness of the transitional layer is assigned as 500 m and 1000 m, which correspond to $h = 1$ and $h = 2$ in the previous section. The variations in the EM fields and current density with depth at a period of 10 s are

presented as an example. Because the lower boundaries of the transitional layer in the two cases are located at depths of 1000 m and 1500 m, only the results at depths ranging from 0 to 2000 m are shown (Section 5 and Figures 6 and 7). The variations in the EM fields and current density with depth for the anisotropic models with dip angles of 15°, 30° and 60° are presented in Section 5 and Figures 6 and 7. To show the attenuation of the EM fields with depth, the EM fields are normalized by the values at the surface of the model. Additionally, in order to more clearly show the influences of the transitional and anisotropic layers rather than the top layer on the current density, the current density was normalized by the electric fields at the surface of the model.

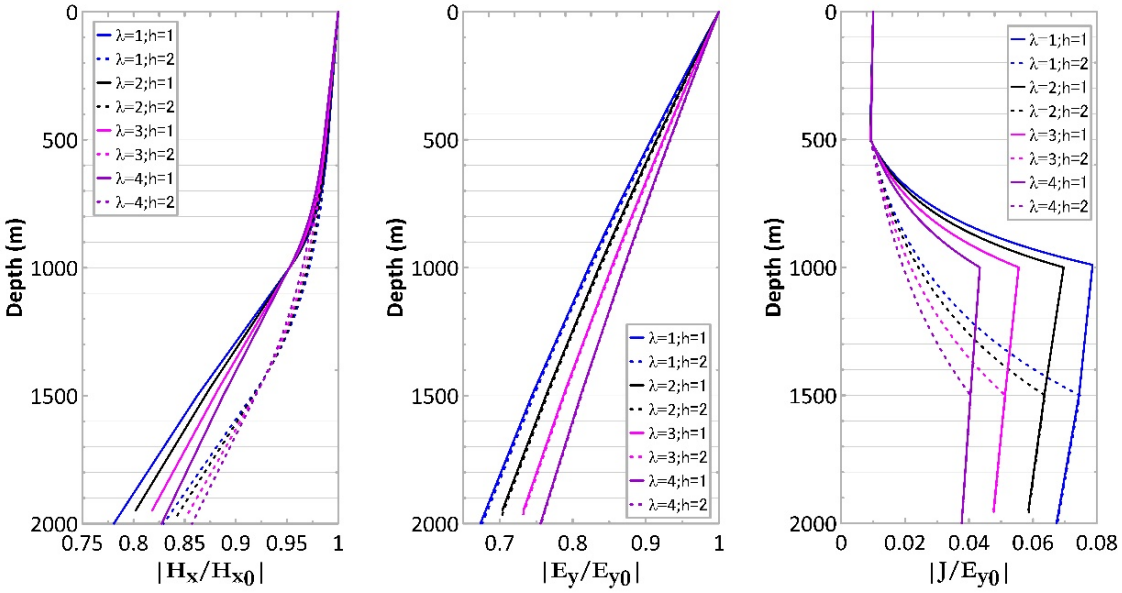

Figure 5. The variation in the amplitude of the normalized magnetic field (left panel), electric field (middle panel) and current density (right panel) with depths ranging from 0 to 2000 m for the anisotropic model with a dip angle of 15° in the bottom layer at a period of 10 s.

The attenuations of the magnetic fields are presented in the left-hand panels in Section 5 and Figures 6 and 7, and the attenuation characteristics are different in different layers. The attenuations are nearly linear with the depth in the first layer, and the differences in the attenuations for different models are indistinguishable and may be neglected when the dip angle is 15° (left-hand panel in Figure 5), and the differences become distinguishable as the angle increases (left-hand panels in Figures 6 and 7). At the approximate depths of the lower boundary of the transitional layer (1000 and 1500 m), the decay curves for different models merge when the dip angle is 15° (left panel in Figure 5) and 30° (left panel in Figure 6). The attenuation of the magnetic fields is strongly affected by the middle layer's thickness.

For the attenuation of the electric field shown in the middle panels in Section 5 and Figures 6 and 7, it is clear that the electric field is always continuous across layers with different conductivities, and the attenuation is approximately linear with depth at 0–2000 m. With the increase in the values of the dip angle in the model, the attenuation of the electric fields decreases, except when the basement layer is isotropic (blue lines). The effect of the middle layer's thickness on the electric fields is negligible.

A comparison of the attenuation of the magnetic fields in the left-hand panels and the electric fields in the middle panels in Section 5 and Figures 6 and 7 also shows that the influence of the transitional and anisotropic layers on the magnetic fields is more significant than that on the electric fields.

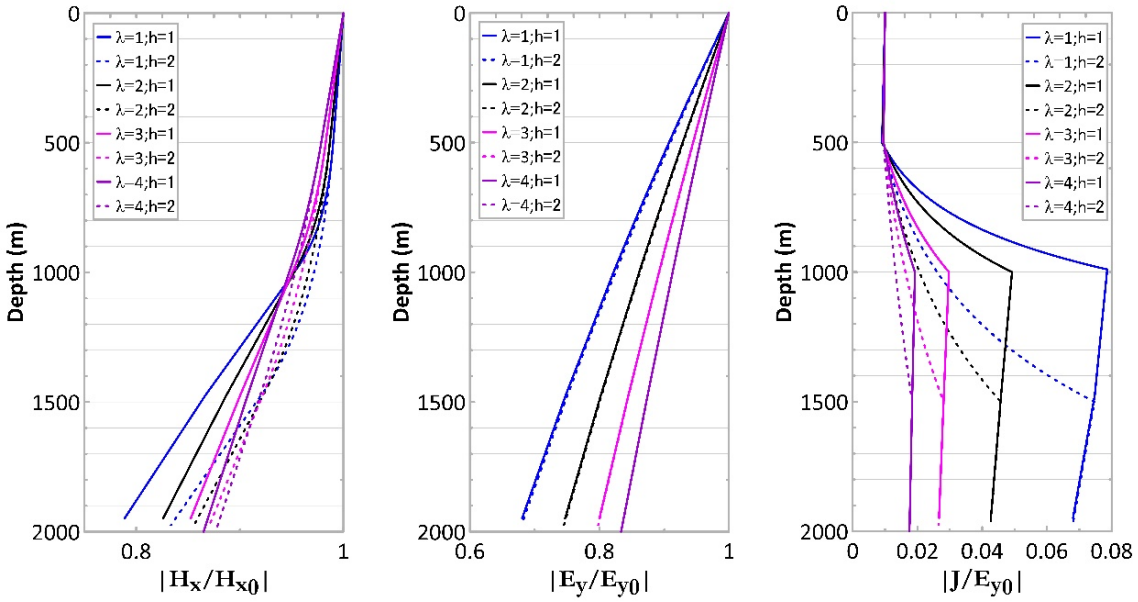

Figure 6. Similar to the case shown in Figure 5 except that the anisotropic dip angle is 30° in the model.

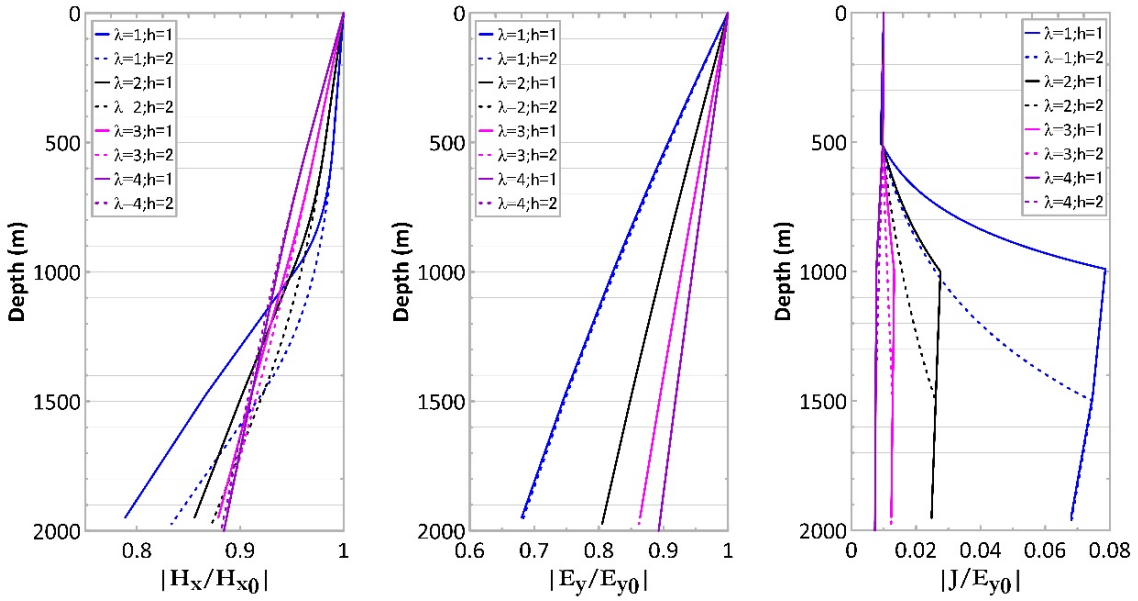

Figure 7. Similar to the case shown in Figure 5 except that the anisotropic dip angle is 60° in the model.

According to Ohm's law ($J = \sigma E$), the current should diffuse at the same rate as the electric field in each layer. However, the magnitude of the current depends on the value of the conductivity of the medium, and therefore, in general, different conductivities always cause different currents at the interfaces between layers. This phenomenon is evident in the right-hand panels in Section 5 and Figures 6 and 7. Of note, the diffusion of the current is almost the same as that in the first layer for these cases.

6. Conclusions

In this work, the EM fields of a 1D stratified model containing a middle transition layer of exponentially varying conductivity with depth were explicitly solved. The conductivity in the transition layer may increase or decrease with depth depending on the conductivity

value in the top and bottom layers. The electric and magnetic fields in the transitional layer are written in the form of modified Bessel functions.

The dependence of the apparent resistivity and impedance phase on the dip angles, anisotropic coefficient and normalized thickness were investigated in detail. The influence of the intensity of anisotropy and dip angle on the current and EM fields was also examined. The attenuation of the electric fields is almost linear with depth, while the attenuation of the magnetic field is nonlinear. The variation of the magnetic fields with depth is strongly affected by the middle layer's thickness and the anisotropic coefficient. The variation in the current density with depth in the transitional layer is similar to the feature of the conductivity. The interfaces between layers are clearly seen from the current density profile.

The obtained results may be useful for studying and understanding the attenuation of the EM fields in the Earth. The simple models may also be convenient for testing computational programs.

Author Contributions: Conceptualization, L.Q.; methodology, L.Q. and C.Y.; validation, L.Q. and W.D.; writing—original draft preparation, L.Q.; writing—review and editing, C.Y. and W.D.; funding acquisition, L.Q. All authors have read and agreed to the published version of the manuscript.

Funding: This work was supported in part by the National Natural Science Foundation of China (grant nos. 42176092 and 41776079) and the Scientific Research Fund of the Second Institute of Oceanography, MNR (grant no. JG2102).

Institutional Review Board Statement: Not applicable.

Informed Consent Statement: Not applicable.

Data Availability Statement: Not applicable.

Acknowledgments: The authors thank Josef Pek, who provided the 1D computer program for validating the algorithm in this study.

Conflicts of Interest: The authors declare no conflict of interest.

Appendix A. Determination of the Unknown Coefficients in Equation (19)

From the last two equations in Equation (19), it is easy to calculate the ratio of the unknown coefficients C and D:

$$\frac{C}{D} = \frac{UNK_1(\gamma_2) + K_0(\gamma_2)}{UNI_1(\gamma_2) - I_0(\gamma_2)} \tag{A1}$$

The ratio of the unknown coefficients A and B may then be expressed in terms of $\frac{C}{D}$ in Equation (A1):

$$\frac{A}{B} = \frac{\left[\frac{C}{D}I_0(\gamma_1) - K_0(\gamma_1)\right] - \left[\frac{C}{D}I_1(\gamma_1) - K_1(\gamma_2)\right]}{\left[\frac{C}{D}I_1(\gamma_1) - K_1(\gamma_2)\right] + \left[\frac{C}{D}I_0(\gamma_1) - K_0(\gamma_1)\right]} \tag{A2}$$

Substitution of Equation (A1) into (A2) yields:

$$\frac{A}{B} = \frac{Q-1}{Q+1}e^{2k_1z_1} \tag{A3}$$

where $Q = \frac{[UNK_1(\gamma_2)+K_0(\gamma_2)]I_0(\gamma_1)+[UNI_1(\gamma_2)-I_0(\gamma_2)]K_0(\gamma_1)}{[UNK_1(\gamma_2)+K_0(\gamma_2)]I_1(\gamma_1)-[UNI_1(\gamma_2)-I_0(\gamma_2)]K_1(\gamma_1)}$

Appendix B. Instructions for the Code Z1ANIS

The program code Z1ANIS used to validate the algorithm in this study was developed by Pek and Santos [59], who stated the mathematical formulation and solution procedure for calculating the impedance of an anisotropic layered medium. For completeness, a short description of the algorithm and instructions for the corresponding code are presented here. Please refer to the original study for more detailed information.

The algorithm was developed on the basis of the method of the impedance propagated through a stack of anisotropic layers. The impedance tensor is propagated from the top of the homogeneous base layer up to the Earth's surface. The corresponding computation program code Z1ANIS was written in Fortran language and attached to the study [59]. Unfortunately, the website server for downloading the source code no longer works, but readers may obtain the source code from the corresponding author.

Here, the instructions for the code are briefly presented. It requires the user to input the number of layers of the medium (NL, including the homogeneous base layer), and four arrays with the layer thicknesses ($H(I), I = 1, 2, \ldots,$ NL; in km), effective principal conductivities ($A_1(I), A_2(I), I = 1, 2, \ldots,$ NL; in S/m) and the effective anisotropy strikes ($\alpha(I), I = 1, 2, \ldots,$ NL; in degrees). For a given period of the EM field t (in seconds), the subroutine gives the impedance tensor on the surface in the form of a 2×2 complex array ($Z(I, J), I, J = 1, 2$; in SI units (Ohm)). The apparent resistivity and impedance phase may then be easily calculated from the surface impedance. The code requires very limited computational resources and can run on any modern computer.

References

1. Cagniard, L. Basic Theory of the MT methods of Geophysical Propecting. *Geophysics* **1953**, *18*, 605–635. [CrossRef]
2. Tikhonov, A.N. The determination of the electrical properties of the deep layers of the earth's crust. *Dokl. Acad. Nauk. SSR* **1950**, *73*, 295–297. (In Russian)
3. Tikhonov, A.N. On determining electrical characteristics of the deep layers of the earth's crust. In *Magnetotelluric Methods*; Vozoff, K., Ed.; Society of Exploration Geophysicists: Tulsa, Oklahoma, 1986; pp. 2–3.
4. Wannamaker, P.E.; Stodt, J.A.; Rijo, L. *PW2D—Finite Element Program for Solution of Magnetotelluric Responses of Two-Dimensional Earth Resistivity Structure*; User Documentation; Earth Sciences Lab-158; Utah University Research Institute: Salt Lake City, UT, USA, 1985.
5. Wannamaker, P.E.; Stodt, J.A.; Rijo, L. A stable finite-element solution for two-dimensional magnetotelluric modeling. *Geophys. J. R. Astron. Soc.* **1987**, *88*, 277–296. [CrossRef]
6. Mackie, R.L.; Madden, T.R.; Wannamaker, P.E. Three-dimensional magnetotelluric modeling using difference equations-Theory and comparisons to integral equation solutions. *Geophysics* **1993**, *58*, 215–226. [CrossRef]
7. Pek, J.; Verner, T. Finite-difference modelling of magnetotelluric fields in two-dimensional anisotropic media. *Geophys. J. Int.* **1997**, *128*, 505–521. [CrossRef]
8. Li, Y.G. A finite-element algorithm for electromagnetic induction in two-dimensional anisotropic conductivity structures. *Geophys. J. Int.* **2002**, *148*, 389–401. [CrossRef]
9. Yang, C. MT numerical simulation of symmetrically 2D anisotropic media based on the finite element method. *Northwest. Seismol. J.* **1997**, *19*, 27–33. (In Chinese)
10. Newman, G.A.; Alumbaugh, D.L. Three-dimensional magnetotelluric inversion using non-linear conjugate gradients. *Geophys. J. Int.* **2000**, *140*, 410–424. [CrossRef]
11. Avdeev, D.; Avdeeva, A. 3D magnetotelluric inversion using a limited-memory quasi-Newton optimization. *Geophysics* **2009**, *74*, F45–F57. [CrossRef]
12. Siripunvaraporn, W.; Egbert, G. WSINV3DMT: Vertical magnetic field transfer function inversion and parallel implementation. *Phys. Earth Planet. Inter.* **2009**, *173*, 317–329. [CrossRef]
13. Egbert, G.D.; Kelbert, A. Computational recipes for electromagnetic inverse problems. *Geophys. J. Int.* **2012**, *189*, 251–267. [CrossRef]
14. Čuma, M.; Gribenko, A.; Zhdanov, M.S. Inversion of magnetotelluric data using integral equation approach with variable sensitivity domain: Application to EarthScope MT data. *Phys. Earth Planet. Inter.* **2017**, *270*, 113–127. [CrossRef]
15. Singh, A.; Dehiya, R.; Gupta, P.K.; Israil, M. A MATLAB based 3D modeling and inversion code for MT data. *Comput. Geosci.* **2017**, *104*, 1–11. [CrossRef]
16. Grayver, A.V. Parallel three-dimensional magnetotelluric inversion using adaptive finite-element method. Part I: Theory and synthetic study. *Geophys. J. Int.* **2015**, *202*, 584–603. [CrossRef]
17. Kordy, M.; Wannamaker, P.; Maris, V.; Cherkaev, E.; Hill, G. 3-D magnetotelluric inversion including topography using deformed hexahedral edge finite elements and direct solvers parallelized on SMP computers–Part I: Forward problem and parameter Jacobians. *Geophys. J. Int.* **2016**, *204*, 74–93. [CrossRef]
18. Kruglyakov, M.; Kuvshinov, A. 3-D inversion of MT impedances and inter-site tensors, individually and jointly. New lessons learnt. *Earth Planets Space* **2019**, *71*, 1–9. [CrossRef]
19. Kruglyakov, M.; Geraskin, A.; Kuvshinov, A. Novel accurate and scalable 3-D MT forward solver based on a contracting integral equation method. *Comput. Geosci.* **2016**, *96*, 208–217. [CrossRef]
20. Seama, N.; Baba, K.; Utada, H.; Toh, H.; Tada, N.; Ichiki, M.; Matsuno, T. 1-D electrical conductivity structure beneath the Philippine Sea: Results from an ocean bottom magnetotelluric survey. *Phys. Earth Planet. Inter.* **2007**, *162*, 2–12. [CrossRef]

21. Ádám, A.; Novák, A.; Szarka, L. Basement depths of 3D basins, estimated from 1D magnetotelluric inversion. *Acta Geod. Geophys. Hung.* **2007**, *42*, 59–67. [CrossRef]
22. Oskooi, B. 1D interpretation of the Magnetotelluric data from Travale Geothermal Field in Italy. *J. Earth Space Phys.* **2006**, *32*, 1–16.
23. Ariani, E.; Srigutomo, W. 1D and 2D occam's inversion of magnetotelluric data applied in Volcano-Geothermal area in Central Java, Indonesia. *J. Phys. Conf. Ser.* **2016**, *739*, 012039. [CrossRef]
24. Lichoro, C.M.; Árnason, K.; Cumming, W. Resistivity imaging of geothermal resources in northern Kenya rift by joint 1D inversion of MT and TEM data. *Geothermics* **2017**, *68*, 20–32. [CrossRef]
25. Marsenić, A. Understanding 1D magnetotelluric apparent resistivity and phase. *J. Electromagn. Waves Appl.* **2020**, *34*, 246–258. [CrossRef]
26. Reddy, I.K.; Rankin, D. Magnetotelluric effect of dipping anisotropies. *Geophys. Prospect.* **1971**, *19*, 84–97. [CrossRef]
27. Loewenth, D.; Landisma, M. Theory for magnetotelluric observations on surface of a layered anisotropic half space. *Geophys. J. R. Astron. Soc.* **1973**, *35*, 195–214. [CrossRef]
28. Shoham, Y.; Loewenthal, D. Magnetotelluric impedance tensor computational for an anisotropic 1-Dimensional layered media. *Geophysics* **1975**, *40*, 155.
29. Kaufman, A.A.; Keller, G.V. *The Magnetotelluric Sounding Method. Methods in Geochemistry and Geophysics*; Elsevier Scientific: Amsterdam, The Netherlands, 1981; Volume 15, p. 596.
30. Yungul, S.H. Magnetotelluric sounding three-layer interpretation curves. *Geophysics* **1961**, *26*, 465–473. [CrossRef]
31. Patella, D. Interpretation of magnetotelluric resistivity and phase soundings over horizontal layers. *Geophysics* **1976**, *41*, 96–105. [CrossRef]
32. Mallick, K. Magnetotelluric sounding on a layered earth with transitional boundary. *Geophys. Prospect.* **1970**, *18*, 738–757. [CrossRef]
33. Srivastav, J.; Niwas, S. Magnetotellurics sounding over models of continuously varying conductivity. *Proc. Natl. Acad. Sci. USA India Sect. A* **1976**, *42*, 320–327.
34. Kao, D.; Rankin, D. Magnetotelluric response on inhomogeneous layered earth. *Geophysics* **1980**, *45*, 1793–1802. [CrossRef]
35. Kao, D. Magnetotelluric Response on Vertically Inhomogeneous Earth. *J. Geophys. Res.* **1981**, *86*, 3027–3038. [CrossRef]
36. Kao, D. Magnetotelluric response on vertically inhomogeneous earth having conductivity varying exponentially with depth. *Geophysics* **1982**, *47*, 89–99. [CrossRef]
37. Banerjee, B.; Sengupta, B.J.; Pal, B.P. Apparent resistivity of a multilayered earth with a layer having exponential variation of conductivity. *Geophys. Prospect.* **1980**, *28*, 430–452. [CrossRef]
38. Peterson, F.L.; Lao, C. Electric well logging of Hawaiian basaltic aquifers. *Groundwater* **1970**, *8*, 11–18. [CrossRef]
39. Spichak, V.V.; Zakharova, O.K. Porosity estimation at depths below the borehole bottom from resistivity logs and electromagnetic resistivity. *Near Surf. Geophys.* **2016**, *14*, 299–306. [CrossRef]
40. Asfahani, J. Porosity and hydraulic conductivity estimation of the basaltic aquifer in Southern Syria by using nuclear and electrical well logging techniques. *Acta Geophys.* **2017**, *65*, 765–775. [CrossRef]
41. Berdichevsky, M.; Dmitriyev, V.; Mershchikova, N. Investigation of gradient media in deep electromagnetic sounding. *1ZV Akad. Nauk SSSR Series Fiz. Zemli* **1974**, *10*, 61–72.
42. Kim, H.-S.; Lee, K. Response of a multilayered earth with layers having exponentially varying resistivities. *Geophysics* **1996**, *61*, 180–191. [CrossRef]
43. Pal, B.P. Magnetotelluric response on a layered earth with non-monotonic resistivity distribution. In *Deep Electromagnetic Exploration*; Narosa Publishing House: New Delhi, India, 1998; pp. 425–431.
44. Berdichevsky, M.N.; Dmitriev, V.I. *Magnetotellurics in the Context of the Theory of Ill-Posed Problems*; Society of Exploration Geophysicists: Tulsa, OK, USA, 2002.
45. Yoshio, K.; Takehiko, K. On the Phase Difference of Earth Current Induced by the Changes of the Earth's Magnetic Field. *Sci. Rep. Tohoku Univ.* **1950**, *2*, 138–141.
46. Qin, L.; Yang, C. Magnetotelluric Soundings on a Stratified Earth with Two Transitional Layers. *Pure Appl. Geophys.* **2020**, *177*, 5263–5274. [CrossRef]
47. Negi, J.G.; Saraf, P.D. Inductive sounding of a stratified earth with transition layer resting on dipping anisotropic beds. *Geophys. Prospect.* **1973**, *21*, 635–647. [CrossRef]
48. Kovacikova, S.; Pek, J. Generalized Riccati equations for 1-D magnetotelluric impedances over anisotropic conductors Part I: Plane wave field model. *Earth Planets Space* **2002**, *54*, 473–482. [CrossRef]
49. Qin, L.; Yang, C.; Ding, W. Magnetotelluric responses of a vertical inhomogeneous and anisotropic resistivity structure with a transitional layer. *Acta Geod. Geophys.* **2022**, *57*, 157–176. [CrossRef]
50. Chlamtac, M.; Abramovici, F. The electromagnetic fields of a horizontal dipole over a vertically inhomogeneous and anisotropic earth. *Geophysics* **1981**, *46*, 904–915. [CrossRef]
51. Zima, L. The Interpretation of Resistivity Sounding over Weathered Rocks. *Geophys. Trans.* **1987**, *32*, 319–332.
52. Sinha, A.K. The magnetotelluric effect in an inhomogeneous and anisotropic earth. *Geoexploration* **1969**, *7*, 9–28. [CrossRef]
53. Cavaliere, T.; Jones, A.G. On the identification of a transition zone in electrical conductivity between the lithosphere and asthenosphere: A plea for more precise phase data. *J. Geophys.* **1984**, *55*, 23–30.
54. Simpson, F.; Bahr, K. *Practical Magnetotellurics*; Cambridge University Press: Cambridge, UK, 2005.

55. Chave, A.D.; Jones, A.G. *The Magnetotelluric Method: Theory and Practice*; Cambridge University Press: Cambridge, UK, 2012.
56. Boas, M.L. *Mathematical Methods in the Physical Sciences*; John Wiley & Sons: Hoboken, NJ, USA, 2006.
57. Persidis, S. *Mathematical Handbook*; ESPI Publishing: Athens, Greece, 2007.
58. Negi, J.; Saraf, P. Impedance of a Plane Electromagnetic Wave at the Surface of a Layered Conducting Earth with Dipping Anisotropy. *Geophys. Prospect.* **1972**, *20*, 785–799. [CrossRef]
59. Pek, J.; Santos, F.A.M. Magnetotelluric impedances and parametric sensitivities for 1-D anisotropic layered media. *Comput. Geosci.* **2002**, *28*, 939–950. [CrossRef]